Chapter 12
Synergy Between Electric Pulse and Thermal Effects

Ravi Joshi

Abstract Generally, in studies of the bioelectric effects of nanosecond pulses, thermal effects are not considered. While this is certainly true for the delivery of single or a small number of pulses, developments in medical treatment based on tissue ablation have been based pulse trains applied at a high repetition rate. In fact, temperature increases may trigger thermally activated bioeffects. This suggests technological opportunities for electro-manipulation that takes advantage of synergisms between thermal and electrically driven processes. Even with modest temperature changes, large thermal gradients could be established, which in itself can lead to additive electric field creation. The focus in this chapter is on thermal aspects and the possible synergies with electrical stimulation for bio-effects.

12.1 Introduction

Most of the literature on the application of high-intensity ultrashort cellular pulses (e.g., Joshi et al. 2005, Song et al. 2011; Pierro et al. 2014; Croce et al. 2010; Camp et al. 2012), has ignored possible thermal effects because of the small (nanosecond) duration of the applied voltage pulses. One potential effect of local temperature enhancements is the increased fluidity of fatty acid tails within the phospholipid bilayer which would facilitate membrane poration (Song et al. 2011). Here we argue that issues associated with local heating should not be entirely dismissed. The importance of locally driven phenomena (such as sectional heating) cannot be overstated, even if globally averaged changes over the entire cell may remain negligible. As an example, rise of temperature induces localized calcium release (termed blips from single channels or puffs from a small collection of channels) can lead to global cellular signaling through a regenerative feedback mechanism (Swillens et al. 1999). More importantly, even if the temperature changes remained small and well controlled (to avoid non-local collateral damage), it is entirely conceivable that *substantial local temperature gradients could be created*.

This issue of differential power dissipation in biological cells, which leads to temperature gradients, was first treated by the Slovenian group (Kotnik and Miklavčič 2000). It was shown that power dissipation within the membrane, becomes much

S. J. Beebe et al., *Ultrashort Electric Pulse Effects in Biology and Medicine*,
Series in BioEngineering, https://doi.org/10.1007/978-981-10-5113-5_12

more pronounced in the MHz and lower GHz regions. In theory, a temperature differential across the outer cell membrane could be maintained by having an electromagnetic pulse-train of relatively short duration of ~ 5 ns (Croce et al. 2010). They demonstrated that temperature differentials across the outer cell membrane in the 5–10 K range were possible. For example, it was shown based on an equivalent lumped-circuit continuum analysis, that ultrashort high-intensity pulses could produce fast localized heating at the cell membrane, with the cytoplasm temperature being essentially unaffected. Physically, this consequence arises from large differences between the conductivity of cell membranes and the cytosol. Peaks of membrane temperature between 1 °C and 5 °C for single 10 ns and 1 ns pulses, respectively, were predicted (Croce et al. 2010). For a typical 5 nm cell membrane, temperature gradients ranging from 0.2×10^9 to 10^9 K/m were reported (Croce et al. 2010). Such possibilities of setting up thermal gradients also arise in the context of pulsed laser irradiation of cells (Garner et al. 2016), and radio-frequency or alternating current electric excitations (Garner et al. 2013). Other specific ways to create temperature gradients include the use of nanoparticles in the vicinity of tumor cells, and subjecting the system to electromagnetic radiation (Chen and Zhang 2006; Richardson et al. 2006), with thermal gradients as large as 10^8 K/m being reported a few years ago (Govorov et al. 2006). With laser excitation, temperature gradients of the order of 10^6 K m^{-1} can routinely be obtained in experiments (Jiang et al. 2009).

The thermoelectric effect is a potentially relevant phenomenon associated with thermal gradients, and involves the development of an electric field. Molecular dynamic (MD) simulations in water have shown that a thermal gradient of 10^{10} K/m can result in the creation of an internal electric field of about 10^8 V/m (Bresme et al. 2008). It was demonstrated that a thermal gradient polarizes water in the direction of the gradient, leading to a non-negligible electrostatic field whose origin lies in the water reorientation under nonequilibrium conditions. More specifically, the hydrogen atoms (or more generally the smaller of the two species in a polar molecule) begins pointing preferentially towards the cold region. Based on simple continuum mechanics, the electrostatic field (E) and the driving temperature gradient (dT/dr) are related as: $E \sim (1 - 1/\varepsilon_r)\,(dT/dr)/T$, where ε_r is the dielectric constant. Hence, the electric field induced by the temperature gradient should be larger for high dielectric constant materials such as water. It is therefore very plausible that the creation of such fields driven by temperature gradients could enhance electroporation in biological cells. This aspect, however, has not been probed to the best of our knowledge. A more subtle point concerns the lifetime of the temperature gradient, and this can be understood from the following argument. When a thermal gradient is applied, the homogeneous system evolves to reduce the entropy production, which is made possible by creating an internal polarization. The heat transfer, which is dominated by intermolecular interactions and molecular polarization, is then reduced (Muscatello et al. 2011). Thus, the polarized system as a whole becomes a less effective heat conductor, implying that any local temperature increase and spatial gradient created would likely be sustained for a longer duration.

In this chapter, we focus on both the thermal heating in the presence of an external electric field to gauge synergistic effects, and also discuss thermal gradients as drivers for electroporative enhancements, even though the actual temperature values might not have changed appreciably from their equilibrium levels. Thus, aspects such as phase changes or protein denaturization are ignored assuming that the absolute temperature changes due to such ultrashort pulses are minimal, around 1–5 °C at most (Pakhomov et al. 2003). Such a study is particularly relevant to high-intensity, nanosecond pulses which are inherently nonthermal in nature, but could establish large thermal gradients.

12.2 Simulation Results with Heating and Electric Pulsing

Analysis of the cellular response to electrical pulses requires an evaluation of the time- and spatial-dependent voltage and current distributions within the cell. This voltage is the source for pore opening and other cellular bio-responses. A possible method to modeling is to represent the electrical characteristics of the cells by a distributed equivalent circuit. Dynamic changes in cell parameters need to be included for self-consistency, since application of the transmembrane voltage can lead to membrane conductance increases over time associated with electroporation.

Details of the numerical distributed circuit approach for computing the spatio-temporal voltages and current flows in cells have already been as discussed in detail earlier in another chapter. Essentially, the entire cell is broken up into discrete segments of resistor–capacitor (RC) circuit elements. The computational region here was taken to be a sphere that included the cell cytoplasm, its plasma membrane, and the surrounding cell-suspension medium. Application of the Kirchhoff current law at each discretized node, then yielded a set of N coupled linear equations in the N node voltages.

Local temperature increases due to dissipation of the electrical energy would be governed by the following thermal diffusion equation: $\delta T/\delta t = (k_T \nabla\ T + E.J)/(\rho_M\ c_M)$, where T is the temperature, k_T the thermal conductivity of the bio-segment, E and J denote the local electric field and current density, respectively, through the membrane. Also, ρ_M is the density, and c_M the membrane specific heat. Over time scales much shorter than those of heat diffusion across the cell (e.g., ~ 200 ns), membrane temperatures will essentially evolve adiabatically. The early times are an important temporal regime since they correspond to intervals during or immediately following the application of electrical pulses. Events triggered by the external fields are being initiated during this time, and so the presence of locally elevated temperatures would work to influence the overall outcomes and kinetic rates, thereby providing synergy to the field-driven processes.

The distributed circuit model was applied to a spherical cell of radius 10 μm consisting of cytoplasm ($\varepsilon = 60\ e_0$, $\sigma = 0.13$ S/m), outer medium ($\varepsilon = 80\ e_0$, $\sigma = 0.6$ S/m), and a 5 nm thick plasma membrane ($\varepsilon = 8\ e_0$, $\sigma = 5.3 \times 10^{-6}$ S/m). The

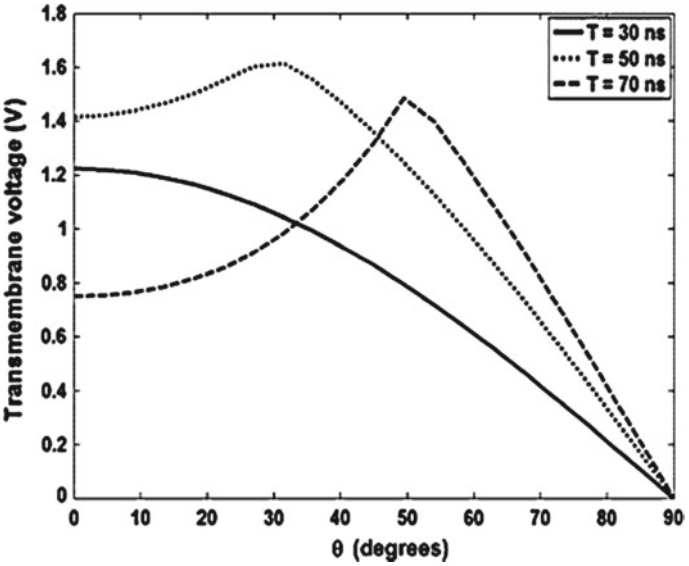

Fig. 12.1 Simulation results for the transmembrane potential versus angular position due to a trapezoidal pulse having a 6 ns rise- and fall-times, and a 60 ns ON time. Values at the three different time instants are shown (after Song et al. 2011)

transmembrane potential as a function of angular location at different time instants is shown in Fig. 12.1.

This result of Fig. 12.1 was in response to a rectangular 60 kV/cm pulse with a 6 ns rise time, a 60 ns ON time and a 6 ns fall time. At the earliest 30 ns snapshot, the potential across the membrane at the poles (i.e., $\theta = 0°$) is predicted to be above 1.2 V. However, as poration at the polar caps initiates, the localized conductivity increases. This leads to a slight lowering of the transmembrane voltage at the polar region as seen in the 50 ns curve. Finally, the 70 ns curve reveals an overall expansion of the porated region around the polar cap.

Changes in local conductivity due to membrane poration were computed, and the values shown in Fig. 12.2. Large increases by orders of magnitude are predicted over time starting at the $\theta = 0°$ location, with the highest conductivity of about 0.007 S/m occurring at the "poles" of the spherical cell. Based on the time-dependent conductivity and transmembrane voltage, the power dissipation density could then be computed.

These power density values are shown in Fig. 12.3 as a function of time for five different angular locations. The initial power dissipation is negligible since the membrane acts as a virtual open circuit with the displacement current being the dominant mechanism. At later times (~ 40 ns and beyond), the conduction current develops as pores begin to form and increase both in density and radial size. Due to the nonlinear increases in conductance and pore densities over time, the power density attains a peak, and then begins to reduce. The decrease can be associated

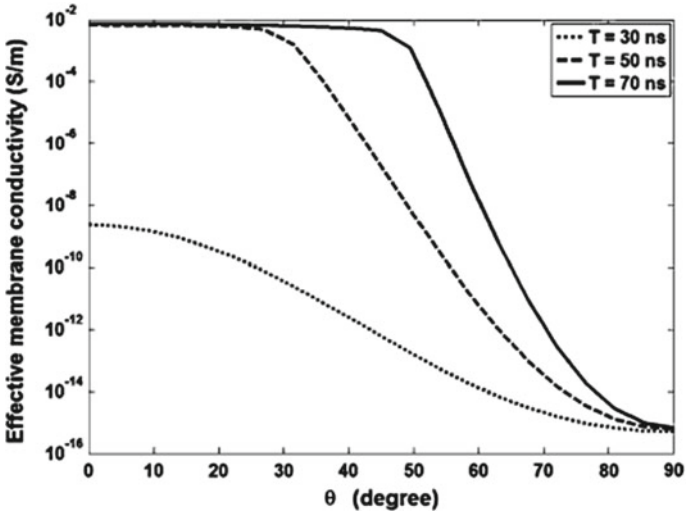

Fig. 12.2 Calculated membrane conductivity versus angular position due to the electrical pulse of Fig. 12.1. Plots at the three different time instants of 30, 50, and 70 ns are shown (after Song et al. 2011)

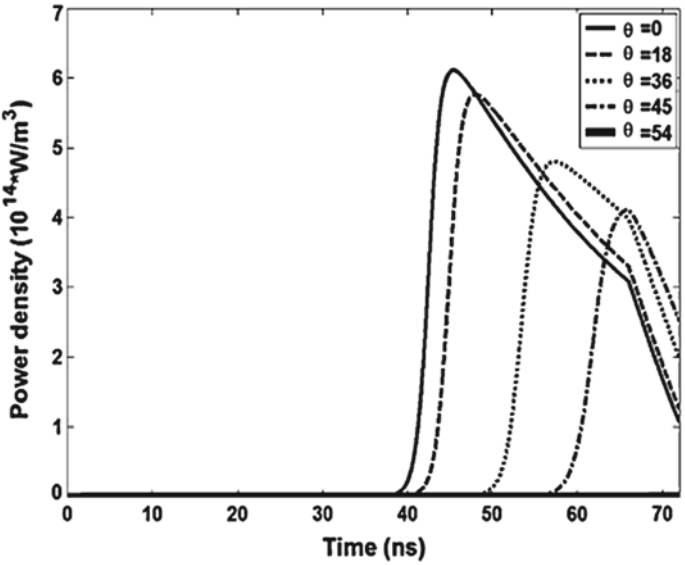

Fig. 12.3 Calculated dissipated power density at the membrane as a function of time. Five different angular locations are shown (after Song et al. 2011)

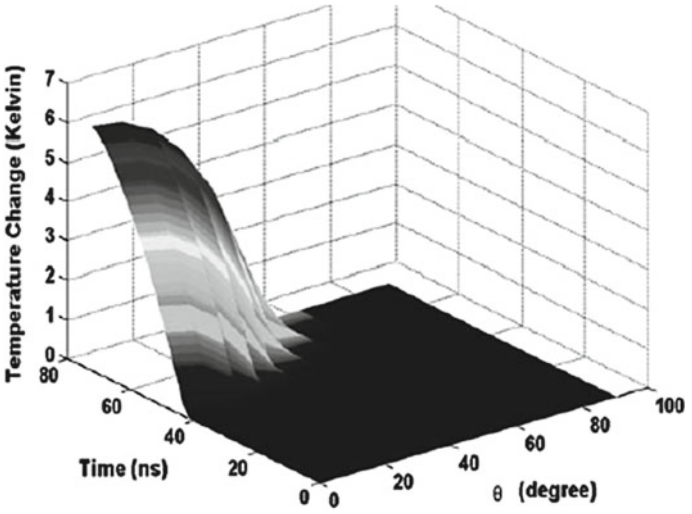

Fig. 12.4 Results for the membrane temperature change as a function of time at different angular locations (after Song et al. 2011)

with a collapse of the local transmembrane potential as the pores effectively produce an electrical "short".

Based on the power density, changes in temperature as a function of time and angular location were obtained next. Values for the density ρ_M and membrane specific heat c_M were chosen to be 10^3 kg/m^3 and 2×10^3 J/kg/K, respectively, in keeping with reports (Croce et al. 2010). Figure 12.4 shows the temperature profile. Interestingly, the largest temperature increase, which occurs at the poles (i.e., $\theta = 0°$), is predicted to have a value of about 6 K. However, a rapid fall-off is seen in Fig. 12.4 away from the poles, with near negligible temperature changes predicted for much of the cell. So, while a near-thermalized situation seems to prevail in an averaged sense, localized heating could be a factor at specific sites. For example, local cellular temperature increases at the membrane could work to energetically enhance procaspase-8 cleavage, and hence promote cellular apoptosis.

As a simple step towards showing that the localized hot spots produced by exposure of cells to ultrashort pulses could then work to accelerate bio-physical processes, we use poration as a demonstrative example. Poration is a well-known cellular effect initiated at the plasma membrane (Neumann et al 1989; Weaver and Chizmadzhev 1996). Heat-induced events at membranes include unfolding of spectrin, redistribution of proteins, and denaturation (Davio and Low 1982; Ivanov 1999). Though these latter processes are relatively slow, application of repetitive pulses could be used as a technique to bring about such temperature-driven changes as well.

Many of the bioprocesses are difficult to model and quantify due to lack of data and parameter values. However, membrane poration can be simulated with a high degree of accuracy based on the MD technique. Hence here, the possible role of localized temperature elevations on electroporation was probed as a simple, yet pertinent, example. Results of MD simulations are shown in Fig. 12.5a, b for a patch of DPPC membrane. The primary objective was to see if temperature increases would foster electro-poration. MD simulations were carried out with a 0.5 V/nm background electric field—one at a temperature of 313 K and the other at 316 K. The trends were consistent, and as seen in the 1 ns snapshot of Fig. 12.5a (which represents a typical simulation outcome), no pore is predicted to form for the 313 K case. However, the simulation at 316 K shows pore formation at the same time instant. Water nanowires connecting the extra- and intra-cellular regions through the membrane are also apparent. The result underscores the role of temperature in facilitating and accelerating the poration process. These results, by showing snapshots of membrane poration at two specific temperatures, point to the possibility that relatively modest variations in temperature generated by exposing cells to electrical pulses, can result in different degrees of bio-effects.

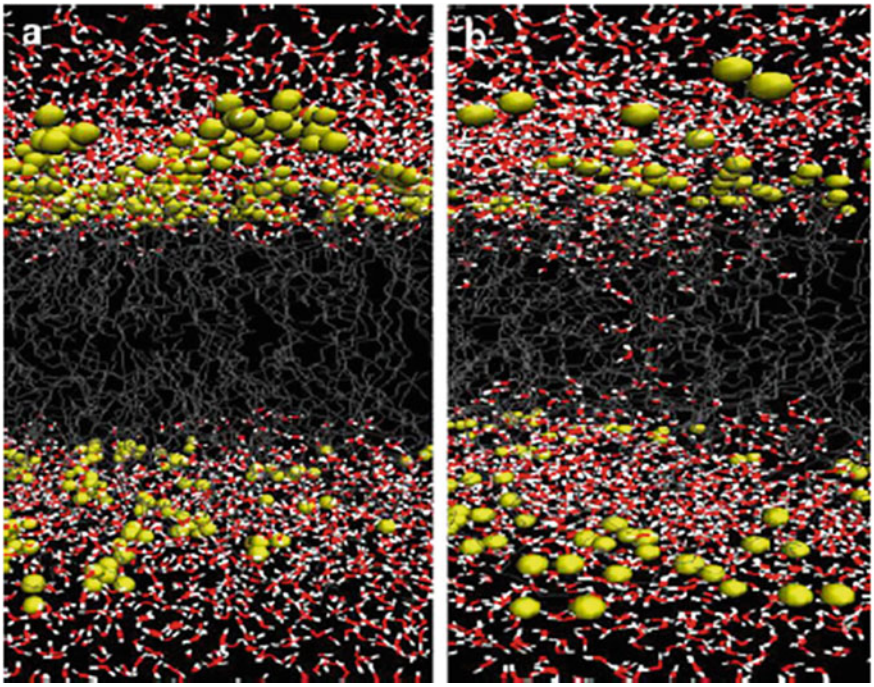

Fig. 12.5 Molecular Dynamics snapshots of the electroporation process in a dipalmitoyl-phosphatidyl-choline (DPPC) membrane under the E field of 0.5 V/nm. Snapshots at 1 ns for two different temperatures of: a 313 K, and b at a temperature of 316 K. A nano-wire forms at the higher temperature (after Song et al. 2011)

Data pertaining to temperature effects (non-electrical in origin) on the mitochondrial membrane are already available (Nijhuis et al. 2006). Experiments on HL60 cells seem to indicate a thermal induction of apoptosis launched by mitochondrial membrane processes involving the Bcl-2 family (Narita et al. 1998). Hence, it is plausible that electrical pulse-induced localized mitochondrial membrane heating could add to several biological outcomes, and so further studies seem warranted. In this regard, experiments on liver cancer cells (Camp et al. 2012) showed enhanced rate of trypan blue uptake (which is indicative of cell death) upon exposure to subnanosecond high electric field pulses, when the temperature was raised above 37 °C. The exposure of Hepa 1–6 cells to 2000 pulses of 200 picosecond duration and electric field amplitudes exceeding 80 kV/cm induced cell death in almost 30% of the cells when the temperature was increased to 47 °C for the time of the pulsing. On the other hand, for temperatures at 37 °C and below, the same exposure to pulsed electric fields did not show any measurable effect. Even for the maximum elevated temperature of 47 °C, thermal effects were not found to cause fatalities for the time of exposure, which was, for 2000 pulses at a repetition rate of 7–9 pulses per second, on the order of 5 min. The use of elevated temperature together with the effect of multiple pulses, was the likely cause for the observed high death rate of the Hepa cells. This hypothesis is in keeping with the results of molecular dynamics simulations presented earlier in this section.

An even more recent report involves the irradiation assisted nanosecond tumor ablation of squamous cancers (Hornef et al. 2020). This recent study showed that nanosecond pulsed electric field cancer therapy may be improved further with the assistance of moderate heating of the target. Heating of the tumor cells was achieved in an integrated manner through a feedback-looped heating system that used a 980-nm fiber optic laser. Synergistic effects between the nanosecond pulsed electric field and the moderately elevated temperature at the target were observed, resulting in enhanced overall survival tumor regression up to 50% in the treatment of lung squamous cell cancer in mice.

12.3 Role of Thermal Gradients

The dynamics of pore formation and water entry into a lipid bilayer membrane with thermal gradients, in response to an externally applied static electric field, was studied (Song et al 2017). Simulations were based on the molecular-dynamics (MD) scheme using the GROMACS package (Berendsen et al. 1995) with a 2 fs time step. Different temperatures were assigned to various regions to simulate the appropriate temperature gradients. The lipid membrane was taken to comprise of dipalmitoyl-phosphatidyl-choline (DPPC) molecules. A constant electric field was used for each simulation, while the top and bottom surfaces of the membrane were assigned two separate fixed values. The water-membrane system contained 6323 water molecules and 128 DPPC lipid molecules in a 6.9 nm $\times$ 7.4 nm $\times$ 7.0 nm simulation box. This

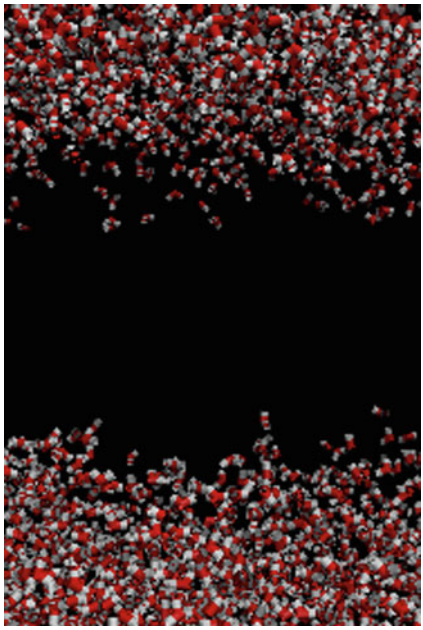

Fig. 12.6 A 7 ns snapshot of DPPC membrane section subject to a constant 0.4 V/nm external electric field. A uniform temperature of 295 K was assumed (after Song et al. 2017)

membrane system was charge-neutral and represents a homogeneous section of a simple lipidic membrane system.

A 7 ns snapshot for a DPPC membrane set at a uniform temperature of 295 K is shown in Fig. 12.6. The central portion represents the membrane, while the water molecules are seen at the top and bottom on the *trans* and *cis* faces. This fixed temperature case serves as a benchmark test case. A high electric field of 0.4 V/nm was applied for these simulations. This high field provides an accelerated test of the bio-physical process of pore formation, since low electric fields would otherwise take inordinately long simulation times. As seen in the 7 ns snapshot of Fig. 12.6 (which represents a typical outcome from a total of six simulation runs starting with different initial velocities), no pore is predicted to form in the membrane. A very slight protrusion at the bottom of the membrane near the middle represents a small and insignificant excursion of the water molecules, but with no beginnings of real pore formation.

To check whether any differences in the outcome may arise due to a temperature gradient, the MD simulations were performed once again on the same geometry, but with the top and bottom membrane surfaces kept at temperatures of and 300 K and 295 K, respectively. A snapshot from the MD simulations at 7 ns showing the molecular structure of the DPPC and water system is given in Fig. 12.7. A nanopore is clearly seen and a water wire is seen to connect the water reservoirs at the top and bottom. The entry of water molecules is slightly stronger at the top, which was the

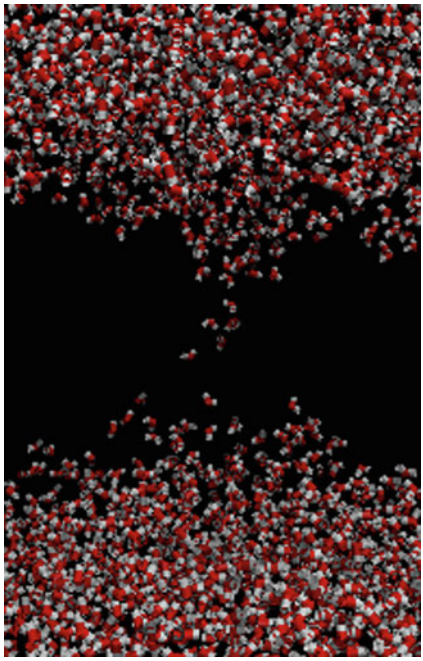

Fig. 12.7 A 7 ns snapshot of DPPC membrane section and the adjoining water molecules subject to a constant 0.4 V/nm external electric field. The membrane temperatures at the top and bottom were maintained at 300 K and 295 K, respectively (after Song et al. 2017)

positive (anode) side and suggests a polarity dependence. This aspect was previously discussed by our group (Hu et al. 2013). It is associated with the molecular stacking of the water network fashioned by the strong external electric field. Basically, in the case of freely rotating molecules, there is competition between energy reduction and the loss of orientational entropy upon alignment which is described by the well-known Langevin equation. For liquid water, orientations of water molecules are also subject to angle restrictions associated with hydrogen bonding and a strong tendency to minimize the loss of hydrogen bonds at the interface (Du et al. 1993; Luzar et al. 1985). The hydrogen bonding between water molecules favors near-parallel dipole orientations relative to the membrane surface upon electric field application. Hence, in order to optimize hydrogen bonding, angular distributions of water molecules relative to the pore walls would be biased against orientations in which the hydrogen atoms point toward the circular walls. This then means that the water would likely enter from the outside at the anode end and move more easily from the inner membrane at the opposite cathode side. The prediction of a faster observable poration from the anode side has indeed been reported experimentally (Vernier et al. 2004).

The difference in pore formation with temperature is again underscored by the results presented in Fig. 12.8a. These MD simulations were carried out at a slightly higher field of 0.45 V/nm and the two snapshots shown were obtained at the longer

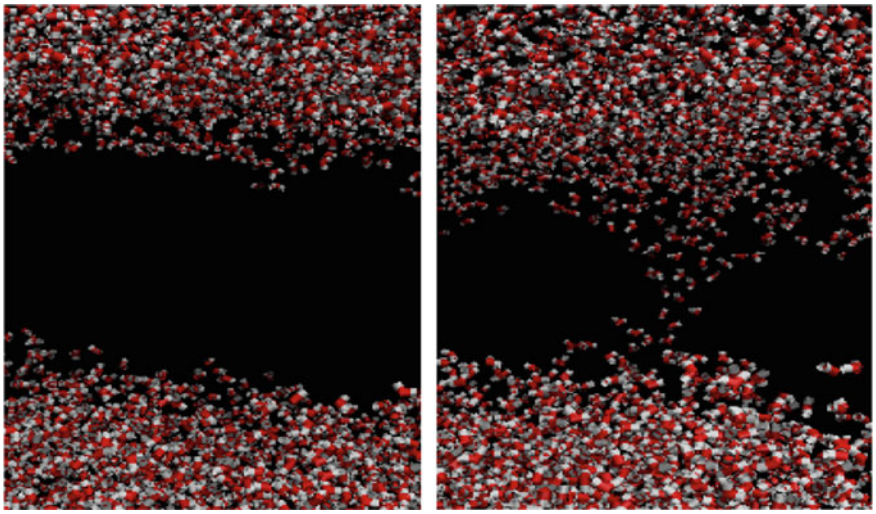

Fig. 12.8 A 10 ns snapshot of a DPPC membrane and the adjoining water molecules at a constant 0.45 V/nm external electric field. **a** Constant temperature of 295 K, and **b** different membrane temperatures at the top and bottom of 300 K and 295 K, respectively (after Song et al. 2017)

10 ns instant. Results shown in Fig. 12.8a were obtained at a constant temperature of 295 K; while for the case shown in Fig. 12.8b, the membrane temperatures at the top and bottom were chosen to be at 300 K and 295 K, respectively. Despite the longer simulation time of 10 ns (as compared to 7 ns for Fig. 12.6) and the higher electric field, no pore formation is evident in Fig. 12.8a. However, in Fig. 12.8b, a nanopore is predicted. The initiation is once again from the upper anode end. Given the 5 nm membrane thickness, this result predicts that the 2×10^9 K/m temperature gradient would synergize electroporation.

The entire mechanism of electric field creation due to internal thermal gradients in water perhaps requires a more detailed explanation and analysis, beyond just numerical MD simulations. This process is best understood in terms of system energy minimization. Assuming near local equilibrium, the solvation energy "G_{sol}" (i.e., the single particle free enthalpy) of a single sphere of diameter "d" is given by: $G_{sol} = -k_B T s d^2$, where k_B is the Boltzmann constant, T the absolute temperature, and "s" a positive constant (Eastman 1926, 1928). Incidentally, the solvation energy G_{sol} is related to the Soret coefficient S_T as: $S_T = [1/(k_B T)]\ \delta G_{sol}/\delta T$, which then leads to: $S_T \sim -s\ d^2$. This Soret effect (also referred to as thermo-migration, or the Ludwig-Soret effect), describes the mass flow induced by a temperature gradient in a fluid (Wiegand 2004), and leads to the following equilibrium equation: $\nabla c + cST\ \nabla T = 0$, with "$c$" being the species concentration.

For the polar water molecules, one can crudely represent this as a dumbbell system having a dipole with two hard spheres of diameters "d_1" and "d_2". Considering such water molecules in a system having a spatial temperature gradient, the overall solvation energy for the molecular system would then be given as: $G_{sol} = -k_B s[T_1 {d_1}^2$

$+ T_2 d_2{}^2]$, where $T_{1,2}$ are the local temperatures at the two sphere 1,2. Physically, the length-scale of temperature variation is much larger than the length of the molecular dumbbell. Mathematically, these temperatures can be expressed in terms of the mean temperature at the midpoint as: $T_{1,2} = T \pm (L/2)\{(T_1 - \mathrm{T}_2)/L\} \equiv T \pm \Delta$, where $L \sim d_1 + d_2$ is the length of the dumbbell, and $T \sim (T_1 + T_2)/2$ is the average temperature in the vicinity of the water molecule. Denoting d_1 to be the diameter of the larger oxygen molecule, and the ratio of the diameters $d_1/d_2 = R$ (i.e., $R > 1$), one gets: $G_{sol} = - k_B s\, d_2{}^2\, [T\, (R^2 + 1) + \Delta\, (R^2 - 1)]$. Clearly for minimizing the energy G_{sol}, one requires $\Delta > 0$. Hence, the temperature T_1 of the molecular system on the side containing the larger oxygen atom would be larger. More generally the smaller of the two species system in the polar molecule would begin pointing preferentially towards the colder region, in the presence of temperature gradients. It may also be pointed out that the effect would be stronger for polar molecules having a larger dipole separation distance L.

In addition to the separation L, the temperature can also be expected to play a role. More generally, the dipoles could be oriented at an angle θ with respect to the applied field direction. In this case then, the average term $\langle \cos(\theta) \rangle = \int_0^\pi \{\cos\,(\theta)\ \sin\,(\theta)\ \exp[-G_{sol}/(k_B T)]\, d\theta\}/\{\int_0^\pi \sin(\theta) \quad \exp[-G_{sol}/(k_B T)] d\theta\}$ would have to be considered. In such a case, lower temperatures would provide a greater likelihood of orientation with the electric field. Also, at higher electric field values, the dipoles could be better aligned and even form a possible lattice structure to enhance the Soret effect. Furthermore, if the outer membrane of a biological cell were subject to electric field pulsing (with or without any additional optical or RF excitation), the outer side would be the hottest. For the cell region facing the anode (e.g., the anodic polar cap), the electronegative oxygen atom of the polar water system would consequently be near the outer membrane, while the hydrogen would be a bit further away. This local polarized field would enhance the total field near the anode pole, and drive cellular electroporation more strongly. This is thus the essence of the additive synergy between a thermal gradient and an applied electric field.

The thermally-induced polarization and development of an associated local electric field can therefore, be seen to be a secondary and synergistic effect, while the primary driver for electroporation is the applied voltage. In fact, it is the electric fields in this case that would cause cellular heating, which would then lead to a differential thermal gradient. The thermal gradient would aid and assist in the electroporation process. In principle, poration at lower electric fields could occur, provided a significantly higher temperature difference is present to drive the process and achieve a comparable result. However practically, there would be two issues with this route: (a) Elevating and then maintaining high temperature gradients would be difficult, and (b) phase transitions could easily occur at the higher temperatures or thermally-activated detrimental cellular effects might be initiated. As a simple example though, simulations at a lower 0.35 V/nm field were carried out with a 15 K thermal gradient, with the outer membrane kept at 310 K. A small "water-wire", can be seen forming in Fig. 12.9 which is a 6.5 ns snapshot. Two different aspects are made obvious from

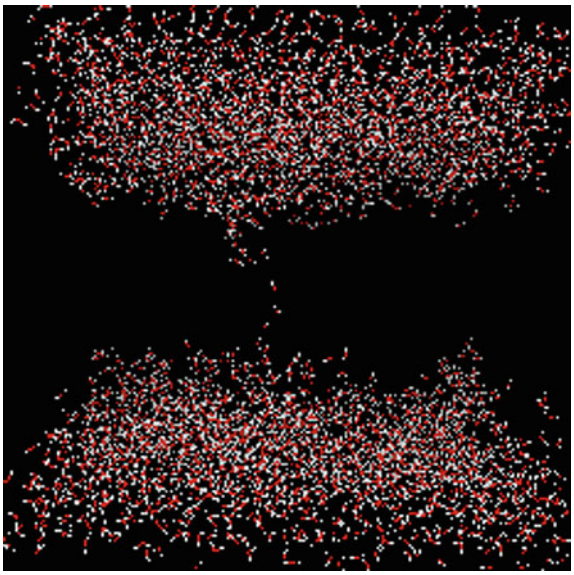

Fig. 12.9 A 6.5 ns snapshot of a DPPC membrane and the adjoining water molecules at a constant 0.35 V/nm external electric field. Different membrane temperatures at the top and bottom of 310 K and 295 K, respectively, were used (after Song et al. 2017)

this result. First, it is possible to electroporate at lower electric fields if higher temperature gradients are used. However, differential values of only up to 10 K have been reported (Pierro et al. 2014), and so maintaining high temperature differentials across membranes would not be easy or practical. Second, the phase transition temperature of DPPC is about 314 K (Leonenko et al. 2004), and so this sets another limit on the differential temperature. Though other much lower electric fields (for example, 0.25 V/nm) were tried for the MD simulations with at most a 313 K temperature for the outer membrane surface (i.e., a 18 K thermal differential), no nanopore formation was observed despite running the simulations up to 15 ns.

In any event, the development of an electrical field due to temperature gradients opens up possibilities for triggering various bio-physical processes for a variety of applications. Here, the role of temperature gradients in facilitating electroporation has been probed. However, other forms of excitation (such as the use of infrared lasers) could also be used to create thermal gradients based on selective and spatially-dependent absorption.

References

Berendsen JC, van der Spoel D, van Drunen R (1995) GROMACS - A Message-passing parallel molecular-dynamics implementation. Comput Phys Commun 95:43–56

Bresme F, Lervik A, Bedeaux D, Kjelstrup S (2008) Water polarization under thermal gradients. Phys Rev Lett 101: 020602/1–4.

Camp JT, Jing Y, Zhuang J, Beebe SJ, Song J, Joshi RP, Schoenbach KH (2012) Cell death induced by subnanosecond pulsed electric fields at elevated temperatures. IEEE Trans Plasma Sci 40:2334–2347

Chen W, Zhang J (2006) Using nanoparticles to enable simultaneous radiation and photodynamic therapies for cancer treatment. J Nanosci Nanotechnol 6:1159–1166

Croce RP, De Vita A, Pierro V, Pinto IM (2010) A thermal model for pulsed EM field exposure effects in cells at nonthermal levels. IEEE Trans Plasma Sci 38:149–155

Davio SR, Low PS (1982) Characterization of the calorimetric C-transition of the human erythrocyte membrane. Biochemistry 21:3575–3582

Du Q, Superfine R, Freysz E, Shen YR (1993) Vibrational spectroscopy of water at the vapor/water interface. Phys Rev Lett 70:2313–2316

Eastman E (1926) Thermodynamics of non-isothermal systems. J Am Chem Soc 48:1482–1493

Eastman E (1928) Theory of the Soret effect. J Am Chem Soc 50:283–291

Garner AL, Deminsky M, Neculaes VB, Chashihin V, Knizhnik A, Potapkin B (2013) Cell membrane thermal gradients induced by electromagnetic fields. J Appl Phys 133:214701/1-11

Garner AL, Neculaes VB, Deminsky M, Dylov DV, Joo C, Loghin ER, Yazdanfar S, Conway KR (2016) Plasma membrane temperature gradients and multiple cell permeabilization induced by low peak power density femtosecond lasers. Biochem Biophys Rep 5:168–174

Govorov AO, Zhang W, Skeini T, Richardson H, Lee J, Kotov NA (2006) Gold nanoparticle ensembles as heaters and actuators: melting and collective plasmon resonances. Nanoscale Res Lett 1:84–90

Hornef J, Edelblute CM, Schoenbach KH, Heller R, Guo S, Jiang C (2020) Thermal analysis of infrared irradiation-assisted nanosecond-pulsed tumor ablation. Sci Rep 10:5122

Hu Q, Zhang Z, Qiu H, Kong M, Joshi RP (2013) Physics of nanoporation and water entry driven by a high-intensity, ultrashort electrical pulse in the presence of cellular hydrophobic interactions. Phys Rev E 87:032704/1-9

Ivanov IT (1999) Investigation of surface and shape changes accompanying the membrane alteration responsible for the heat-induced lysis of human erythrocytes. Colloids Surf B 13:311–323

Jiang HR, Wada H, Yoshinaga N, Sano M (2009) Manipulation of colloids by a nonequilibrium depletion force in a temperature gradient. Phys Rev Lett 102: 208301/1-5

Joshi RP, Hu Q, Schoenbach KH, Beebe SJ (2005) Simulations of transient membrane behavior in cells subjected to a high-intensity ultrashort electric pulse. Phys Rev E 71:031914/1-9

Kotnik T, Miklavčič D (2000) Theoretical evaluation of the distributed power dissipation in biological cells exposed to electric fields. Bioelectromagnetics 21:385–394

Leonenko ZV, Finot E, Ma H, Dahms TES, Cramb DT (2004) Investigation of temperature-induced phase transitions in DOPC and DPPC phospholipid bilayers using temperature-controlled scanning force microscopy. Biophys J 86:3783–3793

Luzar A, Svetina S, Zeks B (1985) Consideration of the spontaneous polarization of water at the solid/liquid interface. J Chem Phys 82:5146–5154

Muscatello J, Romer J, Sala J, Bresme F (2011) Water under temperature gradients: polarization effects and microscopic mechanisms of heat transfer. Phys Chem Chem Phys 13:19970–19978

Narita M, Shimizu S, Ito T, Chittenden T, Lutz RJ, Matsuda H, Tsujimoto Y (1998) Bax interacts with the permeability transition pore to induce permeability transition and cytochrome c release in isolated mitochondria. Proc Natl Acad Sci USA 95:14681–14686

Neumann E, Sowers AE, Jordan CA (1989) Electroporation and electrofusion in cell biology. Plenum Press, New York

Nijhuis EHA, Poot AA, Feijen J, Vermes I (2006) Induction of apoptosis by heat and c-radiation in a human lymphoid cell line; role of mitochondrial changes and caspase activation. Int J Hyperth 22:687–698

Pakhomov AG, Doyle J, Stuck BE, Murphy MR (2003) Effects of high power microwave pulses on synaptic transmission and long term potentiation in hippocampus. Bioelectromagnetics 24:174–181

Pierro V, De Vita A, Croce RP, Pinto IM (2014) Membrane heating in living tissues exposed to nonthermal pulsed EM fields. IEEE Trans Plasma Sci 42:2236–2244

Richardson HH, Hickmaan ZN, Govorov AO, Thomas AC, Zhang W, Kordesch M (2006) Thermooptical properties of gold nanoparticles embedded in ice: characterization of heat generation and melting. Nano Lett 6:783–788

Song J, Garner AL, Joshi RP (2017) Effects of thermal gradients created by electromagnetic fields on cell membrane electroporation probed by molecular dynamics simulations. Phys Rev Appl 7:024003

Song J, Joshi RP, Schoenbach KH (2011) Synergistic effects of local temperature enhancements on cellular responses in the context of high-intensity, ultrashort electric pulses. Med Biol Eng Comput 49:713–718

Swillens S, Dupont G, Combettes L, Champeil P (1999) From calcium blips to calcium puffs: theoretical analysis of the requirements for interchannel communication. Proc Natl Acad Sci 96:13750–13755

Vernier PT, Sun Y, Marcu L, Craft CM, Gundersen MA (2004) Nanoelectropulse-induced phosphatidylserine translocation. Biophys J 86:4040–4048

Weaver JC, Chizmadzhev Y (1996) Theory of electroporation: a review. Bioelectrochem Bioenerg 41:135–160

Wiegand S (2004) Thermal diffusion in liquid mixtures and polymer solutions. J Phys Cond Matt 16:R357–R379